

## Thermal Behaviours of Flower Shape BSA@Cu(II) Hybrid Nanostructures

Burcu Somtürk Yılmaz<sup>1</sup>, Serkan Dayan<sup>2</sup>, Cevahir Altinkaynak<sup>3</sup>, Nilgün Kalaycıoğlu Özpozan<sup>1</sup>, Nalan Özdemir<sup>1\*</sup>

<sup>1</sup>Department of Chemistry, Faculty of Science, Erciyes University, 38039 Kayseri, Turkey

<sup>2</sup>Drug Application and Research Center, Erciyes University, 38280 Kayseri, Turkey

<sup>3</sup>Department of Plant and Animal Production, Avanos Vocational School, Nevşehir Hacı Bektaş Veli University, 50500 Nevşehir, Turkey

\*[ozdemir@erciyes.edu.tr](mailto:ozdemir@erciyes.edu.tr)

\*Orcid: 0000-0002-8930-5198

Received: 16 October 2020

Accepted: 3 March 2021

DOI: 10.18466/cbayarfbe.811643

### Abstract

In this study, flower shape hybrid protein-inorganic hybrid nanostructures were synthesized using a common protein (bovine serum albumin, BSA) and metal ion ( $\text{Cu}^{2+}$ ) at different protein concentrations (0.01, 0.02, 0.05, and 0.1 mg mL<sup>-1</sup>) and pHs (PBS pH:6-9) at +4 °C for investigation of thermal properties the first time in detail. These synthesized protein-inorganic hybrid nanostructures (BSA-Cu<sub>3</sub>(PO<sub>4</sub>)<sub>2</sub>.3H<sub>2</sub>O hNFs) were defined using SEM, EDX, elemental mapping XRD, FTIR, etc. Morphologies of BSA-Cu<sub>3</sub>(PO<sub>4</sub>)<sub>2</sub>.3H<sub>2</sub>O hNFs were characterized by SEM. Element analysis of BSA-Cu<sub>3</sub>(PO<sub>4</sub>)<sub>2</sub>.3H<sub>2</sub>O hNFs was achieved by EDX. Peak positions of BSA-Cu<sub>3</sub>(PO<sub>4</sub>)<sub>2</sub>.3H<sub>2</sub>O hNFs were investigated using XRD. And, the FTIR technique was used to substantiate the creation of hNFs. Also, the thermal behavior such as glass transition and crystallization of BSA-Cu<sub>3</sub>(PO<sub>4</sub>)<sub>2</sub>.3H<sub>2</sub>O hNFs were investigated in detail using thermal gravimetric analysis (TGA).

**Keywords:** BSA, Copper phosphate, Hybrid nanoflowers, Thermal analysis

### 1. Introduction

Protein-inorganic hybrid nanostructures obtained from biomolecules and metal ions are a material that focuses on biological and chemical applications. Furthermore, bioinorganic hybrid nanostructures can show not only a combination of properties of different components but also synergistic properties resulting from the interplay between biological molecules and inorganic substances [1-4]. Because of the unified structural properties and functional practices of biomolecules and nanomaterials, particular attention is paid to the production of bioinorganic hybrids owing to their high composition elasticity and good biocompatibility [5-9].

Nanoflower can be distinguished among nanomaterials by their properties. These nanostructures have attracted the attention of scientists because of the properties of the nano-layers, which let a higher surface-to-volume rate comparatively traditional spherical nanoparticle [10].

Recently there has been a noticeable increase in the synthesis of hybrid nanostructures. In 2012, Zare et al. firstly synthesized the protein-inorganic hybrid nanostructures and reported the formation method of flower-like protein-inorganic hybrid nanostructures using Cu (II) ion as inorganic component and some proteins and enzymes (lactalbumin, laccase, carbonic anhydrase, lipase, and BSA) as an organic component [11]. Flower-shaped hybrid nanostructures are created as a result of a hierarchical unit of nano-sized leaf-shaped structures and growth mechanisms. These nano-sized leaf-shaped structures come together to connect and form structures with flower-like shapes. For this reason, the synthesized structures were named "flower-shaped nanostructures" (Nanoflowers).

In recent years, many studies have been carried out using some small or macromolecules (biomolecules) such as proteins, enzymes, DNA, etc. for synthesis of organic-inorganic hybrid nanomaterials [12-16] Bovine serum albumin (BSA) was used as a protein in some of these studies for different purposes. Yılmaz et al., synthesized BSA-Cu (II) hybrid nanoflowers (BSA-

hNF), and these synthesized structures were used as adsorbents for the detection of cadmium and lead ions in various samples such as hair, food [17]. Zhang et al., synthesized BSA/Zn<sub>3</sub>(PO<sub>4</sub>)<sub>2</sub> hybrid materials. Then, these synthesized structures were used for the adsorption of Cu<sup>2+</sup> [18]. Zhang et al., Mn<sub>3</sub>(PO<sub>4</sub>)<sub>2</sub>@BSA hybrid nanoflower synthesized used as a new support material [19].

Although there are many studies on protein-inorganic hybrid nanoflowers, there are very few studies on the thermal behavior of these hybrid nanoflowers [20, 21]. Song et al. reported a new and easy method for the synthesis of flower-like cobalt phosphate nanocrystals (Co<sub>3</sub>(PO<sub>4</sub>)<sub>2</sub> nanoflowers). Subsequently, they formed an excellent nano biocatalyst system through biomimetic mineralization of cobalt phosphate with Co-type nitrile hydratase (NHase). The encapsulated NHase (NHase@Co<sub>3</sub>(PO<sub>4</sub>)<sub>2</sub>) showed high catalytic efficiencies and stability. They examined the thermal properties of the synthesized nanocrystals. According to the TGA curve, when the temperature rose above 100 °C, there was a sudden tilt due to the water loss of the crystal. However, the NHase@Co<sub>3</sub>(PO<sub>4</sub>)<sub>2</sub> curve fell again in the 200-350 °C range due to the degradation of the proteins, confirming the successful incorporation of NHase. Munyemana et al. synthesized protein-inorganic hybrid materials with hierarchical nanostructures. They used manganese as the inorganic component and collagen as protein. The as-prepared CL-Mn<sub>3</sub>(PO<sub>4</sub>)<sub>2</sub> nanoflowers exhibited good catalytic activity towards water oxidation. At the same time, Thermogravimetric analysis (TGA) was performed under a nitrogen atmosphere, employing a heating rate of 10 °C min<sup>-1</sup> from 25 °C to 500 °C.

The thermal properties of BSA@inorganic hybrid nanostructures (BSA-Cu<sub>3</sub>(PO<sub>4</sub>)<sub>2</sub>.3H<sub>2</sub>O hNFs) have not been studied. In our study, for the first time, the thermal behavior of BSA-Cu<sub>3</sub>(PO<sub>4</sub>)<sub>2</sub>.3H<sub>2</sub>O hybrid nanoflowers was investigated using TGA. At the same time, these synthesized hybrid nanoflowers were characterized by SEM, EDX, FTIR, elemental mapping, and XRD analysis.

## 2. Materials and Methods

### 2.1. Materials

All chemical reagents were analytically pure. Bovine serum albumin (lyophilized powder) and Copper (II) sulfate pentahydrate (CuSO<sub>4</sub>·5H<sub>2</sub>O), potassium phosphate dibasic (KH<sub>2</sub>PO<sub>4</sub>), calcium chloride dihydrate (CaCl<sub>2</sub>·2H<sub>2</sub>O), magnesium chloride (MgCl<sub>2</sub>·6H<sub>2</sub>O), sodium chloride (NaCl), potassium chloride (KCl), sodium phosphate (Na<sub>2</sub>HPO<sub>4</sub>) were obtained from Sigma-Aldrich. In all experiments, pure water was used.

#### 2.1.1. Preparation of flower shape protein-inorganic hybrid nanoflowers (BSA@Cu<sub>3</sub>(PO<sub>4</sub>)<sub>2</sub>.3H<sub>2</sub>O hNFs)

BSA@Cu<sub>3</sub>(PO<sub>4</sub>)<sub>2</sub>.3H<sub>2</sub>O hNFs were fabricated using available methods [22-26]. Initial, CuSO<sub>4</sub>·5H<sub>2</sub>O stock solution (120 mM) was prepared made ready using pure water. Later, certain volume of this solution was added to 8 mL of 10 mM PBS solution (pH:6-9) including at different concentrations BSA (0.01- 0.1 mg/mL). These mixtures were strongly vortexed 30 s and then were incubated for 3 days at 4 °C. Following incubation, each reaction tube was centrifuged throughout for 20 min at 6,500 rpm. Finally, the collected hNFs were dried at room temperature.

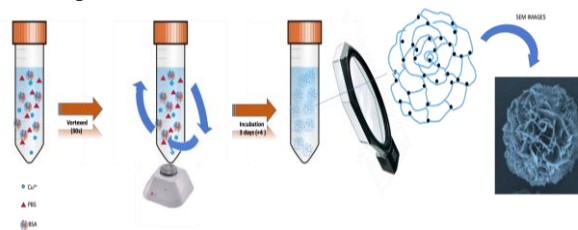


**Fig 1.** A synthesis scheme of BSA@Cu<sub>3</sub>(PO<sub>4</sub>)<sub>2</sub>.3H<sub>2</sub>O hNFs.

#### 2.1.2. Characterization of BSA@Cu<sub>3</sub>(PO<sub>4</sub>)<sub>2</sub>.3H<sub>2</sub>O hNFs

The morphologies of the BSA@Cu<sub>3</sub>(PO<sub>4</sub>)<sub>2</sub>.3H<sub>2</sub>O hybrid nanoflowers were achieved using Scanning electron microscopy (SEM) (ZEISS EVO LS10). The powder diffraction spectra of the synthesized nanoflowers were determined with X-ray diffraction analysis (XRD) (BRUKER AXS D8). For determining weight and atomic percentage of elements such as Cu, N, P, O, Cl in BSA@Cu<sub>3</sub>(PO<sub>4</sub>)<sub>2</sub>.3H<sub>2</sub>O hNFs were used

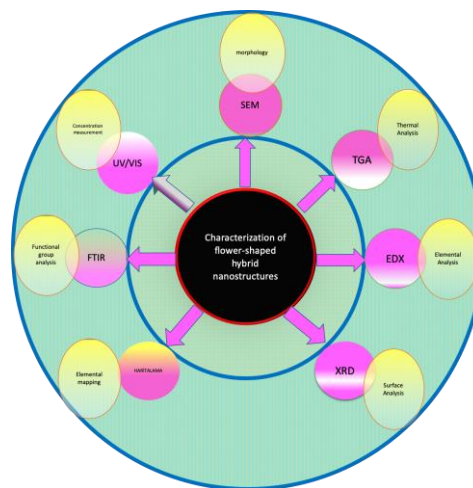


**Fig 2.** Characterization scheme of BSA@Cu<sub>3</sub>(PO<sub>4</sub>)<sub>2</sub>.3H<sub>2</sub>O hNFs.

Energy-dispersive X-ray (EDX) (ZEISS EVO LS10). Bond vibration of hNFs was investigated using the Fourier Transform Infrared Spectroscopy (FTIR) (Perkin Elmer Spectrum 400) spectrum. The thermal properties of BSA@Cu<sub>3</sub>(PO<sub>4</sub>)<sub>2</sub>.3H<sub>2</sub>O hNFs were investigated utilizing TGA (Perkin Elmer Diamond).

### 2.1.3. Determination of thermal properties of BSA@Cu<sub>3</sub>(PO<sub>4</sub>)<sub>2</sub>·3H<sub>2</sub>O hNFs hybrid Nanoflowers

The thermal properties of BSA@Cu<sub>3</sub>(PO<sub>4</sub>)<sub>2</sub>·3H<sub>2</sub>O hNFs were investigated utilizing TGA (Perkin Elmer Diamond). The scanning temperature for each sample was adjusted from 50 °C to 1200 °C (rate of 15 °C min<sup>-1</sup>).

## 3. Results and Discussion

### 3.1. Preparation and characterization of BSA@Cu<sub>3</sub>(PO<sub>4</sub>)<sub>2</sub>·3H<sub>2</sub>O hNFs

BSA@Cu<sub>3</sub>(PO<sub>4</sub>)<sub>2</sub>·3H<sub>2</sub>O hNFs were prepared by mixing Cu<sup>2+</sup> ions and BSA at +4 °C for 3 days in PBS solution (Figure 1). The nucleation and growth phase, which are important in BSA@Cu<sub>3</sub>(PO<sub>4</sub>)<sub>2</sub>·H<sub>2</sub>O hNFs formation, are briefly discussed. In nucleation phase, Cu<sup>2+</sup> ions react with phosphate groups to form copper phosphate nanocrystals. Then, the amine groups in the protein molecules (BSA) are connected to the Cu<sup>2+</sup> ions through the coordination reaction to start nucleation. In the growth phase, anisotropic growth occurs and hNFs are formed completely.

The morphologies and elemental mapping of hNFs were defined using SEM. Chemical and crystal structures of hNFs were defined using FTIR, EDX, and XRD techniques. To sight the formation of nanoflowers, SEM images of the hNFs were taken.

BSA@Cu<sub>3</sub>(PO<sub>4</sub>)<sub>2</sub>·3H<sub>2</sub>O hNFs were synthesized at different pH (pH: 6-10) and concentrations (0.01, 0.02, 0.05 and 0.1, mg mL<sup>-1</sup>) at +4°C. And the differences in the morphology of the synthesized the hNFs were examined by SEM images (Figure 3-7).

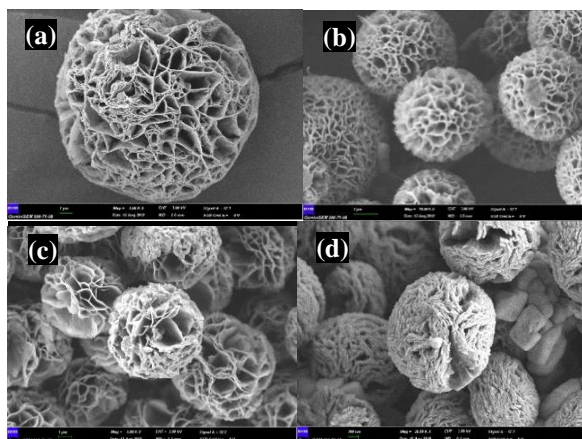


**Fig 3.** SEM images of BSA@Cu<sub>3</sub>(PO<sub>4</sub>)<sub>2</sub>·3H<sub>2</sub>O hNFs prepared at different protein concentrations (pH:6) a) 0.01 mg/mL b) 0.02 mg/mL c) 0.05 mg/mL d) 0.1 mg/mL.

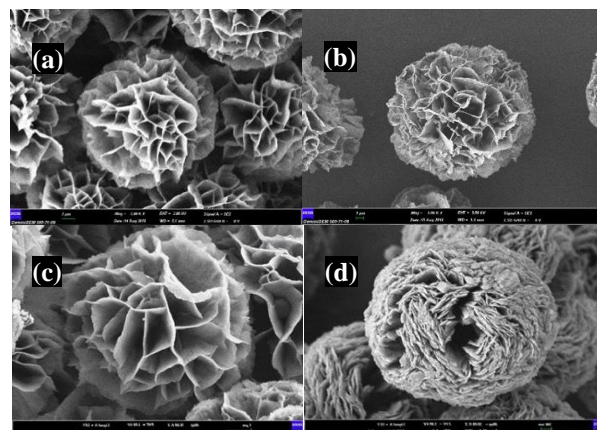


**Fig 4.** SEM images of BSA@Cu<sub>3</sub>(PO<sub>4</sub>)<sub>2</sub>·3H<sub>2</sub>O hNFs prepared at different protein concentrations (pH:7.4) a) 0.01 mg/mL b) 0.02 mg/mL c) 0.05 mg/mL d) 0.1 mg/mL.

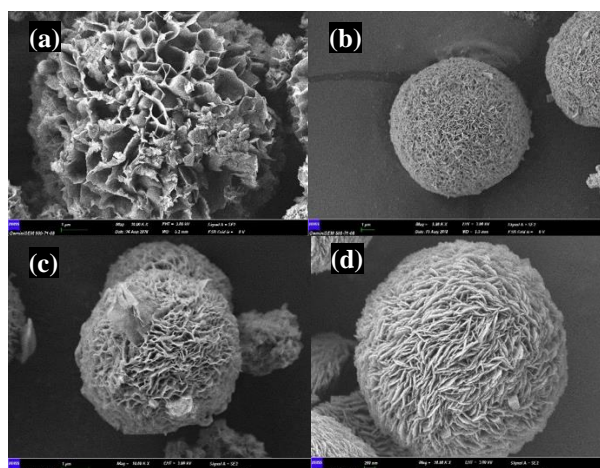


**Fig 5.** SEM images of BSA@Cu<sub>3</sub>(PO<sub>4</sub>)<sub>2</sub>·3H<sub>2</sub>O hNFs prepared at different protein concentrations (pH:8) a) 0.01 mg/mL b) 0.02 mg/mL c) 0.05 mg/mL d) 0.1 mg/mL.

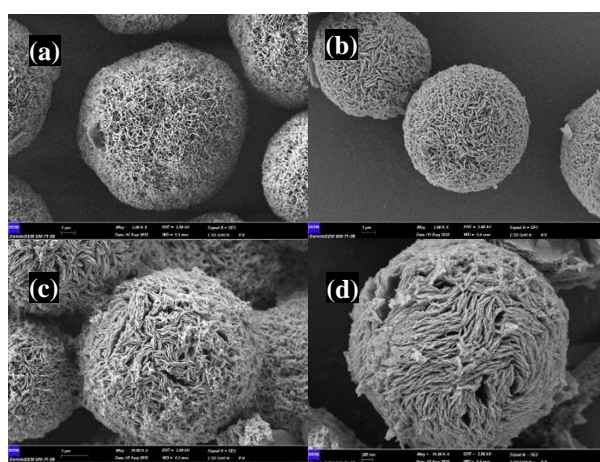


**Fig 6.** SEM images of BSA@Cu<sub>3</sub>(PO<sub>4</sub>)<sub>2</sub>·3H<sub>2</sub>O hNFs prepared at different protein concentrations (pH:9) a) 0.01 mg/mL b) 0.02 mg/mL c) 0.05 mg/mL d) 0.1 mg/mL.

The formations of the  $\text{BSA}@Cu_3(\text{PO}_4)_2 \cdot 3\text{H}_2\text{O}$  hNFs were explored using different concentrations of BSA ( $0.1\text{-}0.01\text{ mg mL}^{-1}$ ) and pHs (pH:6-10). When BSA concentration decreases from 0.1 to  $0.01\text{ mg mL}^{-1}$  were observed significant distinctions in the morphology of  $\text{BSA}@Cu_3(\text{PO}_4)_2 \cdot 3\text{H}_2\text{O}$  hNFs (Fig.3-7). However, as the concentration increased, it showed that all leaves were stiffly intertwined and there were no pores, yet cracks occurred over the surfaces of the  $\text{BSA}@Cu_3(\text{PO}_4)_2 \cdot 3\text{H}_2\text{O}$  hNF for both concentrations. On the surface of the  $\text{BSA}@Cu_3(\text{PO}_4)_2 \cdot 3\text{H}_2\text{O}$  hNFs synthesized in  $0.1\text{ mg mL}^{-1}$  BSA concentration, pores were comparatively formed.  $\text{BSA}@Cu_3(\text{PO}_4)_2 \cdot 3\text{H}_2\text{O}$  hNFs synthesized in  $0.02\text{ mg mL}^{-1}$  and  $0.01\text{ mg mL}^{-1}$  BSA concentrations have quite uniform and spherical pores.

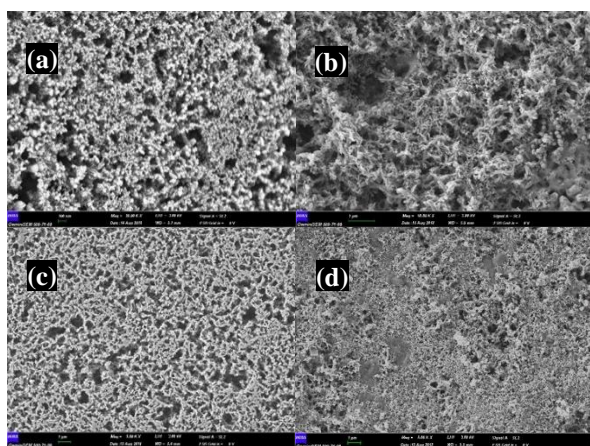


**Fig 7.** SEM images of  $\text{BSA}@Cu_3(\text{PO}_4)_2 \cdot 3\text{H}_2\text{O}$  hNFs prepared at different protein concentrations (pH:10) a)  $0.01\text{ mg/mL}$  b)  $0.02\text{ mg/mL}$  c)  $0.05\text{ mg/mL}$  d)  $0.1\text{ mg/mL}$ .

The effect of pH values (pH 6-9) on the morphology of the  $\text{BSA}@Cu_3(\text{PO}_4)_2 \cdot 3\text{H}_2\text{O}$  hNFs was investigated. The isoelectric point of BSA used in the study is  $\sim 4.5\text{-}5$ , and the protein net charge above or below of this value varies positive and negative. The formation of hybrid nanostructures below pH 5 and above pH 10 did not occur. Since pH is above 10, BSA is loaded with a very negative charge, and pH is under 5, with a very positive charge, protein molecules that are highly positive or highly negative repel each other and as a result of this repulsion, the formation of nanostructures is prevented. EDX analysis of  $\text{BSA}@Cu_3(\text{PO}_4)_2 \cdot 3\text{H}_2\text{O}$  hNFs synthesized at pH 7.4 at different BSA concentrations is shown in figure 8.

The EDX analysis (Fig. 8) of  $\text{BSA}@Cu_3(\text{PO}_4)_2 \cdot 3\text{H}_2\text{O}$  hNFs were performed to determine elemental composition of the hybrid structures. The synthesized HNFs include 2 major components: protein (Bovine serum albumin) and metal phosphate ( $\text{Cu}_3(\text{PO}_4)_2 \cdot 3\text{H}_2\text{O}$ ) nanocrystals. The peak of N and Cu, O and P in the EDX spectrum of the  $\text{BSA}@Cu_3(\text{PO}_4)_2 \cdot 3\text{H}_2\text{O}$  hNFs come from BSA and  $\text{Cu}_3(\text{PO}_4)_2 \cdot 3\text{H}_2\text{O}$  nanocrystals, respectively.

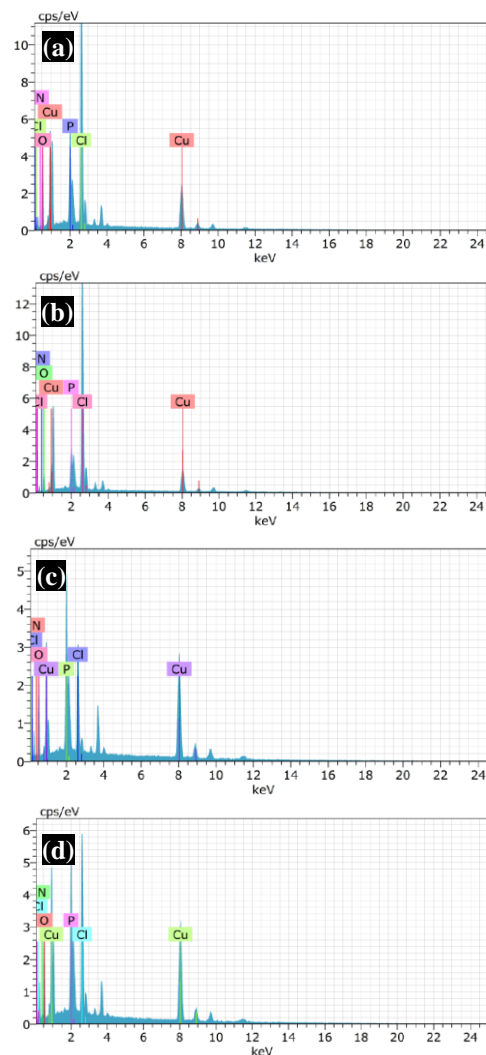


**Fig 8.** EDX analysis of the  $\text{BSA}@Cu_3(\text{PO}_4)_2 \cdot 3\text{H}_2\text{O}$  hNFs synthesized at different BSA concentration a)  $0.01\text{ mg/mL}$ , b)  $0.02\text{ mg/mL}$ , c)  $0.05\text{ mg/mL}$ , d)  $0.1\text{ mg/mL}$ .

**Table 1.** wt % of elements in  $\text{BSA}@Cu_3(\text{PO}_4)_2 \cdot 3\text{H}_2\text{O}$  hNFs synthesized at different concentrations.

Element	wt % of elements at different concentrations			
	0.01 mg/mL	0.02 mg/mL	0.05 mg/mL	0.1 mg/mL
N	%5.23	%5.96	%5.88	%6.88
Cu	%25.25	%25.20	%43.14	%37.64
O	%35.50	%21.49	%24.38	%27.68
P	%10.93	%8.69	%16.46	%13.89

Zeta potential measurements of BSA@Cu<sub>3</sub>(PO<sub>4</sub>)<sub>2</sub>·3H<sub>2</sub>O hNFs were taken. At pH 6, BSA@Cu<sub>3</sub>(PO<sub>4</sub>)<sub>2</sub>·3H<sub>2</sub>O showed a negative load with hNF -19.6 mV zeta potential. The zeta potentials of hNFs at pHs 7.4, 8, and 9 were -27.5 mV, -30.3 mV, and -35.6 mV, respectively.

The chemical structure and formation of the BSA@Cu<sub>3</sub>(PO<sub>4</sub>)<sub>2</sub>·3H<sub>2</sub>O hNFs were appraised by using FTIR (PerkinElmer Spectrum 400). The FTIR spectrum revealed the characteristic peaks of BSA@Cu<sub>3</sub>(PO<sub>4</sub>)<sub>2</sub>·3H<sub>2</sub>O hNFs (Fig. 9).

The FTIR spectrum revealed BSA@Cu<sub>3</sub>(PO<sub>4</sub>)<sub>2</sub>·3H<sub>2</sub>O hNFs characteristic peaks (Figure 9). The bending vibrations of O = P = O groups were observed between ~535 cm<sup>-1</sup> and ~557 cm<sup>-1</sup>. P = O and P-O stretching bands appeared at ~926 cm<sup>-1</sup> and ~979 cm<sup>-1</sup>. The typical BSA's vibration bands at ~1520-1640 cm<sup>-1</sup> belong to the NH<sub>2</sub> groups and the stretching bands at 3048-3300 cm<sup>-1</sup> are connected to the CH<sub>2</sub> and CH<sub>3</sub> groups.

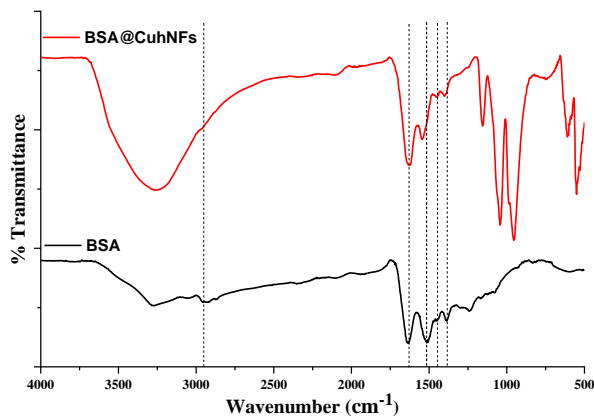


**Fig 9.** FTIR spectra of BSA and BSA@Cu<sub>3</sub>(PO<sub>4</sub>)<sub>2</sub>·3H<sub>2</sub>O hNFs.

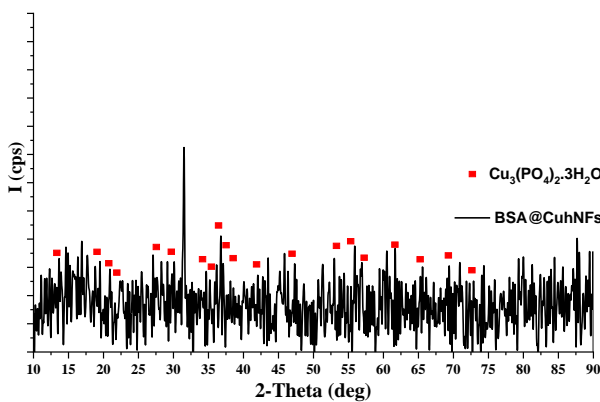


**Fig 10.** X-ray diffraction patterns of BSA@Cu<sub>3</sub>(PO<sub>4</sub>)<sub>2</sub>·3H<sub>2</sub>O hNFs [black line, Cu<sub>3</sub>(PO<sub>4</sub>)<sub>2</sub>·3H<sub>2</sub>O, JCPDS card (00-022-0548)].

Also, BSA@Cu<sub>3</sub>(PO<sub>4</sub>)<sub>2</sub>·3H<sub>2</sub>O hNFs were characterized using XRD analysis (Fig. 10). The crystal structure of hNFs were brighten with the diffraction peaks of Cu<sub>3</sub>(PO<sub>4</sub>)<sub>2</sub>·3H<sub>2</sub>O in the BSA@Cu<sub>3</sub>(PO<sub>4</sub>)<sub>2</sub>·3H<sub>2</sub>O hNFs, which were compatible with them of JCPDS card (00-022-0548).

It is seen from Fig. 11, Cu, N, O, and P elements are homogeneously distributed inside the BSA@Cu<sub>3</sub>(PO<sub>4</sub>)<sub>2</sub>·3H<sub>2</sub>O hNFs

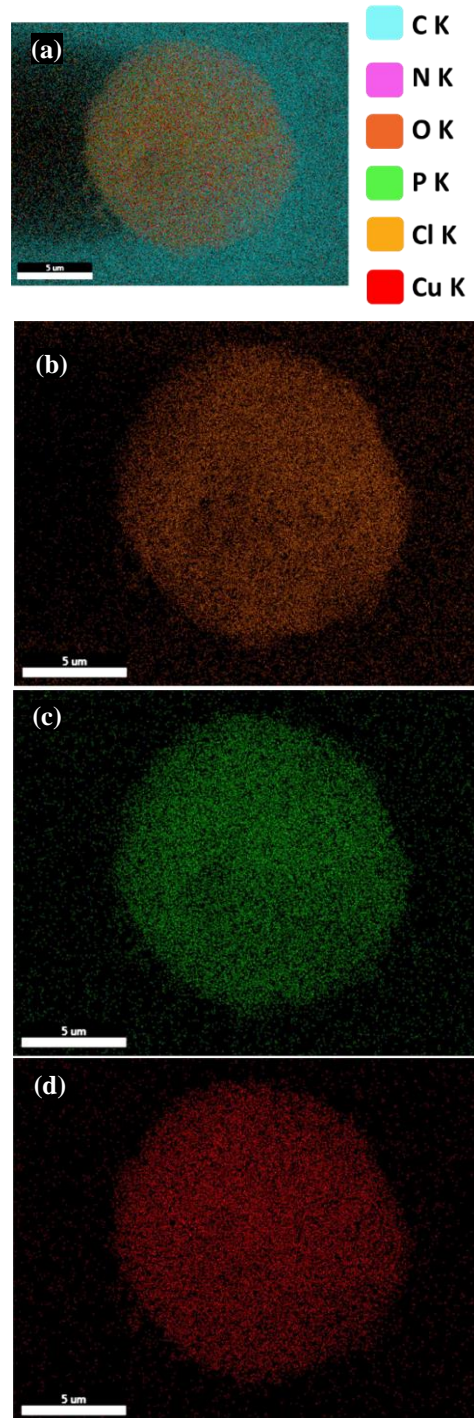


**Fig 11.** Elemental mapping of BSA@Cu<sub>3</sub>(PO<sub>4</sub>)<sub>2</sub>·3H<sub>2</sub>O hNFs a) mix, b) O, c) P, d) Cu

### 3.2. Thermal Studies of BSA@Cu<sub>3</sub>(PO<sub>4</sub>)<sub>2</sub>.3H<sub>2</sub>O hNFs

Thermal analysis studies were performed to confirm the optimum conditions of the fabricated hybrid nanoflowers at different concentrations of BSA and pH.

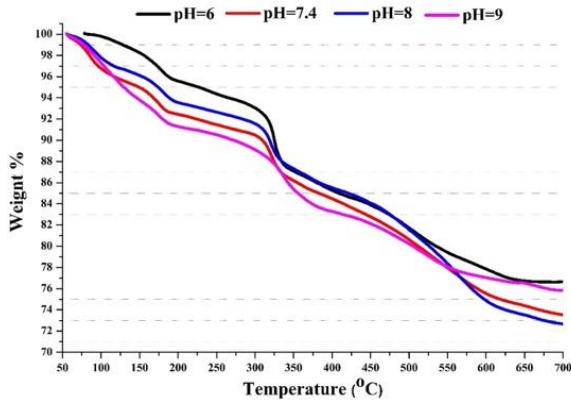


**Fig 12.** TGA results of the synthesized BSA@Cu<sub>3</sub>(PO<sub>4</sub>)<sub>2</sub>.3H<sub>2</sub>O hNFs with different pH at 0.01 mg/mL BSA concentration.

**Table-2.**TGA data of the synthesized BSA@Cu<sub>3</sub>(PO<sub>4</sub>)<sub>2</sub>.3H<sub>2</sub>O hNFs (0.01 mg/mL)

Hybrid Nanoflowers	Step	DTG <sub>max</sub> / °C	T <sub>on</sub> <sup>o</sup> C	T <sub>end</sub> <sup>o</sup> C	Mass loss/ %
BSA@Cu <sub>3</sub> (PO <sub>4</sub> ) <sub>2</sub> .3H <sub>2</sub> O hNFs (0.01mg/mL), pH=6	I	133	78.6	214.3	4.72
	II	324	214.3	353.3	8.32
	III	506	353.3	644.6	10.19
	IV	-	644.6	700.0	0.12
BSA@Cu <sub>3</sub> (PO <sub>4</sub> ) <sub>2</sub> .3H <sub>2</sub> O hNFs (0.01mg/mL), pH=7.4	I	93	61.7	122.6	3.79
	II	167	122.6	204.9	3.46
	III	318	204.9	362.4	6.67
	IV	524	362.4	636.9	11.05
	V	-	636.9	700.0	1.12
BSA@Cu <sub>3</sub> (PO <sub>4</sub> ) <sub>2</sub> .3H <sub>2</sub> O hNFs 0.01mg/mL), pH=8	I	102	63.2	128.9	3.11
	II	173	128.9	221.4	3.53
	III	316	221.4	373.1	6.79
	IV	516	373.1	623.4	12.34
	V	-	623.4	700.0	1.39
BSA@Cu <sub>3</sub> (PO <sub>4</sub> ) <sub>2</sub> .3H <sub>2</sub> O hNFs (0.01mg/mL), pH=9	I	131	58.6	212.8	8.70
	II	314	212.8	389.3	7.60
	III	489	389.3	573.2	6.22
	IV	-	573.2	700.0	1.45

\* T<sub>on</sub> – thermal degradation onset temperature, T<sub>max</sub> – maximum weight loss temperature, T<sub>end</sub> – final thermal degradation temperature

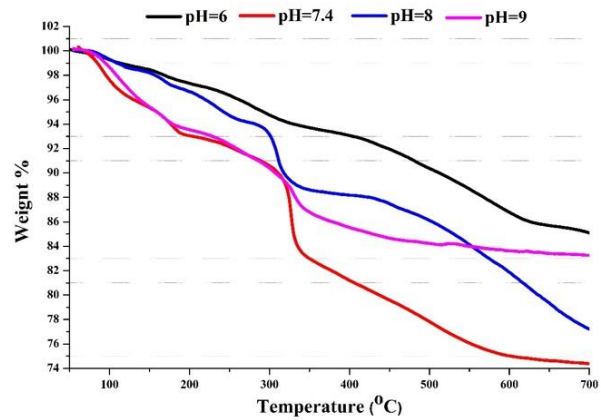


**Fig 13.** TGA results of the synthesized BSA@Cu<sub>3</sub>(PO<sub>4</sub>)<sub>2</sub>.3H<sub>2</sub>O hNFs with different pH at 0.02 mg/mL BSA concentration.

**Table-3.**TGA data of the synthesized BSA@Cu<sub>3</sub>(PO<sub>4</sub>)<sub>2</sub>.3H<sub>2</sub>O hNFs (0.02 mg/mL)

Hybrid Nanoflowers	Step	DTG <sub>max</sub> / °C	T <sub>on</sub> <sup>o</sup> C	T <sub>end</sub> <sup>o</sup> C	Mass loss/ %
BSA@Cu <sub>3</sub> (PO <sub>4</sub> ) <sub>2</sub> .3H <sub>2</sub> O hNFs (0.02mg/mL), pH=6	I	231	68.5	360.9	6.30
	II	528	360.9	643.9	7.80
	III	-	643.9	700.0	0.68
BSA@Cu <sub>3</sub> (PO <sub>4</sub> ) <sub>2</sub> .3H <sub>2</sub> O (0.02mg/mL), pH=7.4	I	109	73.6	120.3	3.36
	II	180	120.3	220.0	3.62
	III	322	220.0	366.8	10.41
	IV	498	366.8	611.7	7.46
	V	-	611.7	700.0	0.53
BSA@Cu <sub>3</sub> (PO <sub>4</sub> ) <sub>2</sub> .3H <sub>2</sub> O (0.02mg/mL), pH=8	I	194	81.2	253.6	5.31
	II	304	253.6	351.9	6.00
	III	545	351.9	700.0	11.39
BSA@Cu <sub>3</sub> (PO <sub>4</sub> ) <sub>2</sub> .3H <sub>2</sub> O (0.02mg/mL), pH=9	I	125	86.5	200.8	5.97
	II	272	200.8	356.3	6.95
	III	485	356.3	700.0	3.32

\* T<sub>on</sub> – thermal degradation onset temperature, T<sub>max</sub> – maximum weight loss temperature, T<sub>end</sub> – final thermal degradation temperature

According to SEM analysis and literature information, BSA@Cu<sub>3</sub>(PO<sub>4</sub>)<sub>2</sub>.3H<sub>2</sub>O hNFs in the optimum conditions were prepared as pH:7.4 and 0.02 mg/ml BSA concentration. Of course, this result was obtained to obtain the nanoflower structure in a smooth morphology and we determined the thermal behavior of the same materials in this study. The pH values were used as 6, 7.4, 8, and 9, as well as, the BSA concentrations were also screened as 0.01, 0.02, 0.05, and 0.1 mg/ml. Also, thermal decomposition steps and thermal degradation onset temperature (T<sub>on</sub>), and final thermal degradation temperature (T<sub>end</sub>) of decomposition temperatures were determined. The screening temperature range for

materials degraded in 4 steps as generally was carried out between 50 to 700 °C. The common result of all thermal curves is that the degradation steps of the materials produced at pH 7.4 are more pronounced and orderly and, the irregularities in thermal curves were observed with increasing BSA concentration

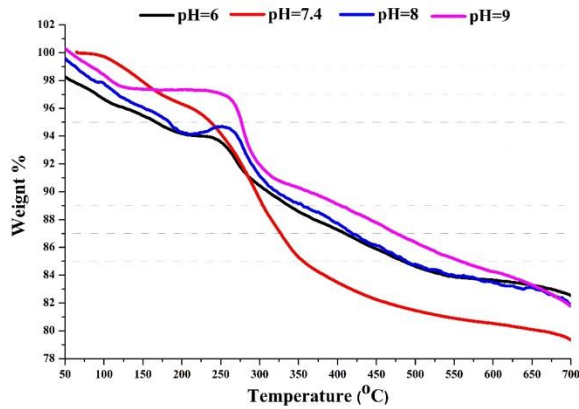


**Fig 14.** TGA results of the synthesized BSA@Cu<sub>3</sub>(PO<sub>4</sub>)<sub>2</sub>.3H<sub>2</sub>O hNFs with different pH at 0.05 mg/mL BSA concentration.

**Table-4.** TGA data of the synthesized BSA@Cu<sub>3</sub>(PO<sub>4</sub>)<sub>2</sub>.3H<sub>2</sub>O hNFs (0.05 mg/mL)

Hybrid Nanoflowers	Step	DTG <sub>max</sub> / °C	T <sub>on</sub> <sup>o</sup> C	T <sub>end</sub> <sup>o</sup> C	Mass loss/ %
BSA@Cu <sub>3</sub> (PO <sub>4</sub> ) <sub>2</sub> .3H <sub>2</sub> O (0.05mg/mL), pH=6	I	120	57.4	202.1	3.84
	II	261	202.1	295.5	3.52
	III	387	295.5	539.8	6.67
	IV	540	539.8	700.0	1.45
BSA@Cu <sub>3</sub> (PO <sub>4</sub> ) <sub>2</sub> .3H <sub>2</sub> O (0.05mg/mL), pH=7.4	I	141	85.5	197.9	3.54
	II	288	197.9	437.6	13.86
	III	482	437.6	700.0	3.20
BSA@Cu <sub>3</sub> (PO <sub>4</sub> ) <sub>2</sub> .3H <sub>2</sub> O (0.05mg/mL), pH=8	I	127	52.5	204.6	5.23
	II	287	204.6	339.3	4.80
	III	517	339.3	700.0	7.57
BSA@Cu <sub>3</sub> (PO <sub>4</sub> ) <sub>2</sub> .3H <sub>2</sub> O (0.05mg/mL), pH=9	I	88	57.3	124.1	2.43
	II	283	124.1	347.9	7.22
	III	546	347.9	700.0	8.59

\* T<sub>on</sub> – thermal degradation onset temperature, T<sub>max</sub> – maximum weight loss temperature, T<sub>end</sub> – final thermal degradation temperature

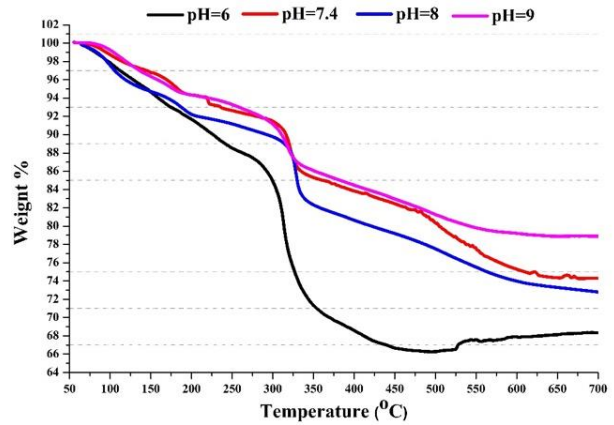


**Fig 15.** TGA results of the synthesized BSA@Cu<sub>3</sub>(PO<sub>4</sub>)<sub>2</sub>.3H<sub>2</sub>O hNFs with different pH at 0.1 mg/mL BSA concentration.

**Table-5.** TGA data of the synthesized BSA@Cu<sub>3</sub>(PO<sub>4</sub>)<sub>2</sub>.3H<sub>2</sub>O hNFs (0.1 mg/mL)

Hybrid Nanoflowers	Step	DTG <sub>max</sub> / °C	T <sub>on</sub> <sup>o</sup> C	T <sub>end</sub> <sup>o</sup> C	Mass loss/ %
BSA@Cu <sub>3</sub> (PO <sub>4</sub> ) <sub>2</sub> .3H <sub>2</sub> O (0.1mg/mL), pH=6	I	164	68.3	250.6	11.45
	II	313	250.6	354.2	17.52
	III	425	354.2	700.0	2.64
BSA@Cu <sub>3</sub> (PO <sub>4</sub> ) <sub>2</sub> .3H <sub>2</sub> O (0.1 mg/mL), pH=7.4	I	176	74.8	267.8	7.60
	II	320	267.8	409.5	8.66
	III	524	409.5	700.0	9.29
BSA@Cu <sub>3</sub> (PO <sub>4</sub> ) <sub>2</sub> .3H <sub>2</sub> O (0.1 mg/mL), pH=8	I	97	64.3	129.8	4.45
	II	180	129.8	220.5	3.66
	III	327	220.5	366.9	10.08
	IV	497	366.9	700.0	8.90
BSA@Cu <sub>3</sub> (PO <sub>4</sub> ) <sub>2</sub> .3H <sub>2</sub> O (0.1 mg/mL), pH=9	I	135	76.7	201.3	5.69
	II	304	201.3	359.5	8.56
	III	473	359.5	700.0	6.84

\* T<sub>on</sub> – thermal degradation onset temperature, T<sub>max</sub> – maximum weight loss temperature, T<sub>end</sub> – final thermal degradation temperature

According to the obtained thermal analyses data, the TGA degradation step took place generally in the IV - V step and the decomposition temperatures were obtained in approximately the same regions for all nanomaterials. Then, the TG curve of the selected BSA@Cu<sub>3</sub>(PO<sub>4</sub>)<sub>2</sub>.3H<sub>2</sub>O hNFs (0.02 mg/mL) material for the most ideal nanoflower production was realized similar to the others. Also, the produced hNFs at pH 7.4 were noted to have more regular and gradual degradation among themselves.

#### 4. Conclusion

Herein, flower shape hybrid protein-inorganic nanostructures (BSA-Cu<sub>3</sub>(PO<sub>4</sub>)<sub>2</sub>. 3H<sub>2</sub>O hNFs) were synthesized using BSA and Cu<sup>2+</sup> ions at different protein concentrations and pHs at +4 °C. This synthesized BSA-Cu<sub>3</sub>(PO<sub>4</sub>)<sub>2</sub>.3H<sub>2</sub>O hNFs were defined using SEM, EDX, elemental mapping XRD, FTIR, etc. Also, using thermal gravimetric analysis (TGA) was investigated by the thermal behavior of nanoflowers. Thermal analyses of the synthesized BSA@Cu<sub>3</sub>(PO<sub>4</sub>)<sub>2</sub>.3H<sub>2</sub>O hNFs were examined as a detailed parameter.

#### Acknowledgement

This study was conducted at the Department of Chemistry, Erciyes University, and was supported by Erciyes University Scientific Research Projects Unit with the project coded FDK-2016-6637.

#### Author's Contributions

**Burcu Somtürk Yılmaz:** Conceptualization, Methodology, Validation, Formal analysis, Investigation, Writing - original draft, Writing - review & editing.

**Serkan Dayan:** Conceptualization, Methodology, Validation, Formal analysis, Investigation, Writing - original draft, Writing - review & editing.

**Cevahir Altınkaynak:** Conceptualization, Methodology, Validation, Formal analysis, Investigation, Writing - original draft, Writing - review & editing.

**Nilgün Kalaycıoğlu Özpozan:** Conceptualization, Methodology, Validation, Formal analysis, Investigation, Writing - original draft, Writing - review & editing.

**Nalan Özdemir:** Conceptualization, Methodology, Validation, Formal analysis, Investigation, Writing - original draft, Writing - review & editing, Supervision. Project administration, Funding acquisition.

#### Ethics

There are no ethical issues after the publication of this manuscript.

#### References

1. Cui, J, Jia, S, Organic-inorganic hybrid nanoflowers: A novel host platform for immobilizing biomolecules. *Coordination Chemistry Reviews*, 2017, 352, 249–263.
2. Shcharbin, D, Halets-Bui, I, Abashkin, V, Dzmitruk, V, Loznikova, S, Odabaşı, M, Acet, Ö, Önal, B, Özdemir, N, Shcharbina, N, Bryszewska, M, Hybrid metal-organic nanoflowers and their application in biotechnology and medicine *Colloids and Surfaces B: Biointerfaces*, 2019, 182, 110354.
3. Talens-Perales, D, Fabra, M, Martínez-Argente, L, Marín-Navarro, J, Polaina, J, Recyclable thermophilic hybrid protein-

inorganic nanoflowers for the hydrolysis of milk lactose. *International Journal of Biological Macromolecules*, 2020, 15, 602–608.

4. Salehiabar, M, Nosrati, H, Javani, E, Aliakbarzadeh, F, Manjili, H.K, Davaran, S, Danafar, H, Production of biological nanoparticles from bovine serum albumin as controlled release carrier for curcumin delivery, *International Journal of Biological Macromolecules*, 2018, 115, 83–89.
5. Zoubi, W, Muhammad, K, Siti, F, Nisa, N, Young, G, Recent advances in hybrid organic-inorganic materials with spatial architecture for state-of-the-art applications *Progress in Materials Science*, 2020, 112, 100663.
6. Zhang, L, Jin, F, Zhang, T, Zhang, L, Xing, J, Structural influence of graft and block polycations on the adsorption of BSA. *International Journal of Biological Macromolecules*, 2016, 85, 252-257.
7. Nosrati, H, Rakhshbahar, A, Salehiabar, M, Afroogh, S, Manjili, H, Danafar, H, Davaran, S, Bovine serum albumin: An efficient biomacromolecule nanocarrier for improving the therapeutic efficacy of chrysin *Journal of Molecular Liquids*, 2018, 271, 639–646.
8. Canepa, J, Torgerson, J, Kim, D.K, Lindahl, E, Takahashi, R, Whitelock, K, Heying, M, Wilkinson, S.P, Characterizing osmolyte chemical class hierarchies and functional group requirements for thermal stabilization of proteins. *Biophysical Chemistry*, 2020, 264, 106410.
9. Zeng, X, Liu, G, Tao, W, Ma, Y, Zhang, X, He, F, Pan, J, Mei, L, Pan, G, A drug-selfgated mesoporous antitumor nanoplatform based on pH-sensitive dynamic covalent bond, *Advanced Functional Materials*, 2017, 27, 160-178.
10. Zhu, J, Niu, Y, Li, Y, Gong, Y, Shi, H, Huo, Q, Liu, Y, Xu, Q, Stimuli-responsive delivery vehicles based on mesoporous silica nanoparticles: recent advances and challenges. *Journal of Mathematical Chemistry B*, 2017, 5, 1339–1352.
11. Ge, J, Lei, J, Zare, R.N, Protein inorganic hybrid nanoflowers. *Nature Nanotechnology*, 2012, 7, 428-432.
12. Zhang, B, Li, P, Zhang, H, Wang, H, Li, X, Tian, L, Ali, N, Ali, Z, Zhang, Q, Preparation of lipase/Zn<sub>3</sub>(PO<sub>4</sub>)<sub>2</sub> hybrid nanoflower and its catalytic performance as an immobilized enzyme, *Chemical Engineering Journal*, 2016, 29, 287–297.
13. Gulmez, C, Altınkaynak, C, Özdemir, N, Atakisi, O, Proteinase K hybrid nanoflowers (P-hNFs) as a novel nanobiocatalytic detergent additive, *International Journal of Biological Macromolecules*, 2018, 119, 803–810.
14. Wu, T, Yang, Y, Cao, Y, Song, Y, Xu, L, Zhang, X, Wang, S, Bioinspired DNA-Inorganic Hybrid Nanoflowers Combined with a Personal Glucose Meter for Onsite Detection of miRNA, *ACS Applied Materials & Interfaces*, 2018, 10, 42050–42057.
15. Dayan, S, Altınkaynak, C, Kayaci, N, Doğan, Ş.D, Özdemir, N, Kalaycıoğlu Özpozan, N, Hybrid nanoflowers bearing tetraphenylporphyrin assembled on copper(II) or cobalt(II) inorganic material: A green efficient catalyst for hydrogenation of nitrobenzenes in water, *Applied Organometallic Chemistry*, 2020, 34(3), 5381.
16. Aydemir, D, Geçili, F, Özdemir, N, Ulusu, N.N, Synthesis and characterization of a triple enzyme-inorganic hybrid nanoflower (TrpE@ihNF) as a combination of three pancreatic digestive enzymes amylase, protease and lipase, *Journal of Bioscience and Bioengineering*, 2020, 129(6), 679-686.
17. Yılmaz, E, Ocsoy, I, Ozdemir, N, Soylak, M, Bovine serum albumin-Cu(II) hybrid nanoflowers: An effective adsorbent for

solid phase extraction and slurry sampling flame atomic absorption spectrometric analysis of cadmium and lead in water, hair, food and cigarette samples. *Analytica Chimica Acta*, 2016, 906, 110-117.

18. Zhang, H, Wang, T, Zheng, Y, Yan, C, Gu, W, Ye, L, Comparative toxicity and contrast enhancing assessments of  $Gd_2O_3@BSA$  and  $MnO_2@BSA$  nanoparticles for MR imaging of brain glioma. *Biochemical and Biophysical Research Communications*, 2018, 499, 488-492.
19. Zhang, Z, Zhang, Y, He, L, Yang, Y, Liu, S, Wang, M, Fang, S, Fu, G, A feasible synthesis of  $Mn_3(PO_4)_2@BSA$  nanoflowers and its application as the support nanomaterial for Pt catalyst. *Journal of Power Sources*, 2015, 284, 170-177.
20. Song, Y, Gao, J, He, Y, Zhou, L, Ma, L, Huang, Z, Jiang, Y, Preparation of a Flowerlike Nanobiocatalyst System via Biomimetic Mineralization of Cobalt Phosphate with Enzyme. *Industrial & Engineering Chemistry Research*, 2017, 56, 14923-14930.
21. Munyemanai J, He, H, Ding, S, Yin, J, Xi, P, Xiao, J, Synthesis of manganese phosphate hybrid nanoflowers by collagen-templated biomineralization. *RSC Advances*, 2018, 8, 2708.
22. Noma, S.A.A, Somtürk Yılmaz, B, Ulu, A, Özdemir, N, Ateş, B, Development of l-asparaginase@hybrid Nanoflowers (ASNase@HNFs) Reactor System with Enhanced Enzymatic Reusability and Stability. *Catalytic Letters*, 2020, DOI: <https://doi.org/10.1007/s10562-020-03362-1>
23. Somturk, B, Yılmaz, I, Altinkaynak, C, Karatepe, A, Ozdemir, N, Ocsöy, I, Synthesis of urease hybrid nanoflowers and their enhanced catalytic properties. *Enzyme and Microbial Technology*, 2016, 86, 134-142.
24. Somturk, B, Hancer, M, Ocsöy, I, Özdemir, N, Synthesis of copper ion incorporated horseradish peroxidase-based hybrid nanoflowers for enhanced catalytic activity and stability, *Dalton Transactions*, 2015, 44, 13845–13852.
25. Altinkaynak, C, Gulmez, C, Atakisi, O, Özdemir, N, Evaluation of organic-inorganic hybrid nanoflower's enzymatic activity in the presence of different metal ions and organic solvents. *International Journal of Biological Macromolecules*, 2020, 164, 162-171.
26. Altinkaynak, C, Kocazorbaz, E, Özdemir, N, Zihnioglu, F, Egg white hybrid nanoflower (EW-hNF) with biomimetic polyphenol oxidase reactivity: Synthesis, characterization and potential use in decolorization of synthetic dyes. *International Journal of Biological Macromolecules*, 2018, 109, 205–211.